Liquid Crystals
Publication details, including instructions for authors and subscription information:
http://www.informaworld.com/smpp/title~content=t713926090

Observation of the tumbling instability in torsional shear flow of a nematic liquid crystal with $\alpha_3 > 0$

T. Carlsson[a]; K. Skarp[a]
[a] Institute of Theoretical Physics and Physics Department, Chalmers University of Technology, S-412 96, Göteborg, Sweden

To cite this Article Carlsson, T. and Skarp, K.(1986) 'Observation of the tumbling instability in torsional shear flow of a nematic liquid crystal with $\alpha_3 > 0$', Liquid Crystals, 1: 5, 455 — 471
To link to this Article: DOI: 10.1080/02678298608086269
URL: http://dx.doi.org/10.1080/02678298608086269

LIQUID CRYSTALS, 1986, VOL. 1, NO. 5, 455–471

Observation of the tumbling instability in torsional shear flow of a nematic liquid crystal with $\alpha_3 > 0$

by T. CARLSSON and K. SKARP
Institute of Theoretical Physics and Physics Department,
Chalmers University of Technology, S-412 96 Göteborg, Sweden

(*Received 3 March 1986; accepted 30 June 1986*)

The shear flow behaviour of the nematic liquid crystal 4-*n*-octyl-4′-cyanobiphenyl (8CB) was studied in a torsional shear flow apparatus. Experiments were performed near the smectic A–nematic phase transition, and they concentrated on the observation of the tumbling instability associated with a positive Leslie viscosity α_3. From theoretical considerations presented here this instability is expected to occur for rather small director tilts when $\alpha_3 \gg |\alpha_2|$. Furthermore a functional dependence of the tumbling instability threshold on the parameter $\alpha_3/|\alpha_2|$ is presented and evaluated experimentally for the nematic 8CB. Good agreement is found between these theoretical results from the Leslie–Ericksen continuum theory and the experimental measurements.

1. Introduction

The study of the dynamical properties of nematic liquid crystals started in the 1920s with attempts by Oseen [1] and Anzelius [2] to develop a hydrodynamical theory of nematics. It was, however, not until after the work by Ericksen [3] and Leslie [4, 5] some 30 years later that a useful hydrodynamical continuum theory of nematics was presented. Leslie showed that for a complete description of the flow properties of nematics six viscosity coefficients are needed. These are commonly denoted by α_i ($i = 1$–6). Later Parodi [6] showed by an Onsager relation that out of the six Leslie coefficients four are linearly dependent, still leaving five viscosity coefficients for the experimentalist to determine.

In order to discuss the qualitative features of nematic flows however only two of the six Leslie viscosities are of importance; these are α_2 and α_3 [7]. For rod-like nematics α_2 is found to be always negative while α_3 can adopt both positive or negative values. For disc-like nematics on the other hand α_2 is also expected to be positive [8, 9]. We shall deal exclusively with rod-like nematics throughout this paper. The flow behaviour of the system is divided into two cases depending on the sign of α_3. In order to discuss these two flow regimes, let us focus our attention to the experimental situation of simple shear flow which is pictured in figure 1. The liquid crystal is confined between two glass plates, distance d apart, both parallel to the xy plane. The lower plate is at rest while the upper one is moving with the velocity v_0 in the x direction. The director is characterized by the polar angles θ and φ shown in the figure.

The case of negative α_3 leads to the well-known situation of flow alignment, i.e. the director will everywhere in the bulk of the sample (for large enough shearing rates) adopt a forward angle to the normal to the plates given by $\arctan\sqrt{(\alpha_2/\alpha_3)}$, still being within the plane of shear ($\varphi = 0$). Only in two thin boundary layers will the director

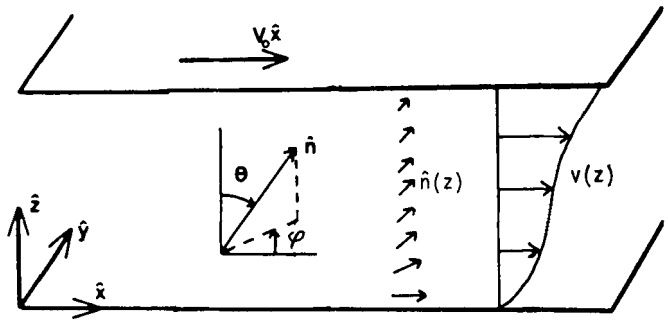

Figure 1. The geometry of the shear flow problem. The liquid crystal is confined between two glass plates, both parallel to the xy plane, distance d apart. The lower plate is at rest while the upper one is moving in the x direction with velocity v_0. The director is characterized by the polar angles θ and φ where θ is the angle between the director and the z axis and φ is the angle between the projection of the director into the xy plane and the x axis.

deviate from this angle due to the boundary conditions which are imposed from the surrounding glass plates.

When α_3 is positive no flow alignment occurs and the situation becomes more complicated. Several different kinds of instabilities have been found to be exhibited in this case. Cladis and Torza (Couette flow) [10, 11] and Pieranski *et al.* [12, 13] (linear shear flow) have shown how, at a critical shearing rate, the director configuration goes through a discontinuous transition, all the time remaining within the plane of shear. This instability has been called a tumbling instability in the literature. The work by Pieranski *et al.* [13] also reported that at a larger shearing rate, the director became unstable with respect to fluctuations which brought it out of the shearing plane (the so-called 'out-of-plane instability'); this instability was not observed by Cladis and Torza [10]. This apparent contradiction is easily resolved by the study of the hydrodynamic torque maps, recently introduced by Carlsson [7]. Instabilities in oscillatory shear flow of nematics have been reported by Clark *et al.* [14]. By performing a torsional shear flow experiment, Skarp *et al.* [15] found some periodic structures which are reviewed in §2.

Theoretical considerations of the shear flow of nematics in the case of positive α_3 have been given by Pikin [16], Manneville [17], Carlsson [7, 18] and Högfors and Carlsson [19]. In one paper [18] Carlsson solves the visco-elastic equations numerically and demonstrates that tumbling is a natural consequence of the mathematical structure of the Leslie–Ericksen equations. In the paper by Högfors and Carlsson criteria for the thresholds of the onset of tumbling as well as the out-of-plane instability are derived analytically.

It is the purpose of this paper to show how the periodic structures which are reported to occur in torsional shear flow for positive α_3 [15] can be explained as a consequence of tumbling. The outline of the paper is as follows. In §2 the concept of torsional shear flow is discussed and the structures observed in [15] are reviewed. In §3 we discuss the tumbling instability in view of [18, 19]. We show here, by a qualitative argument, how the structures which are discussed in §2 can be explained as a consequence of tumbling. In §4 we discuss the present experiment, which is a more systematic repetition of the experiment which is reported in [15]. We give a brief discussion of the relaxation of the system into its time-independent state and we also

show how observation between crossed polarizers can be used as a probe of the stationary director configurations. In §5 we show that by making a reasonable assumption for the temperature dependence of the relevant material parameters we can explain the experimental observations also quantitatively as a consequence of tumbling by solving the equations governing the flow.

2. Flow phenomena in torsional shear flow of nematics with $\alpha_3 > 0$

Assuming the director to be within the plane of shear, i.e. the plane spanned by the velocity and the velocity gradient (the xz plane in figures 1 and 2), the shearing torque acting upon the director is given by

$$\Gamma_y^s = u'(\alpha_3 \sin^2\theta - \alpha_2 \cos^2\theta), \tag{1}$$

where $u' = dv_x/dz$ is the shearing rate. By aligning the director initially along the velocity direction ($\theta = \pi/2$), there are two possible ways for the director to rotate under the influence of the shear (cf. figure 2). If the upper plate is given a shear pulse to the right, the director will be rotated by a shearing torque $\Gamma_y^s = \alpha_3 u'$, which is negative for $\alpha_3 < 0$ (cf. figure 2 (*b*)) and positive for $\alpha_3 > 0$ (cf. figure 2 (*c*)). Since the rotation of the director is easily detected optically, the experiment described can be used to determine the sign of α_3 for a given nematic substance.

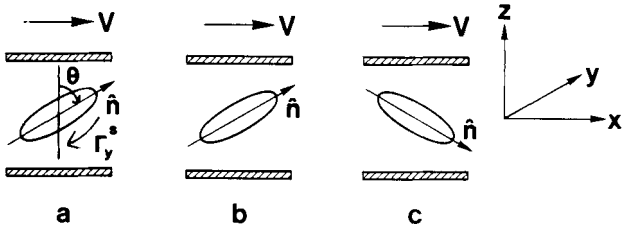

Figure 2. (*a*) Definition of the shear torque Γ_y^s. (*b*) Rotation of an initially parallel director when $\alpha_3 < 0$. (*c*) Rotation of an initially parallel director when $\alpha_3 < 0$.

In order to determine the sign of α_3 for members of the homologous series of cyanobiphenyls

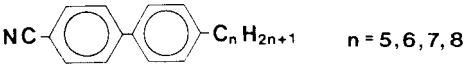

a small flow cell was constructed [15]. In order to obtain the necessary initial alignment (director parallel to the velocity vector), the glass plates were coated with silicon monoxide through evaporation. The flow cell was enclosed in a small temperature chamber, and mounted in a conoscopic optical arrangement, as shown in figure 3. The conoscopic interference pattern, consisting of hyperbolas, moves in the direction of the velocity in case (*c*), and in the opposite direction in case (*b*). By observing the conoscopic pattern when the nematic is given a shear pulse, the sign of α_3 is determined unambiguously.

It was found that α_3 is negative for the first three members of the series in their nematic ranges (although only half of the interval, above room temperature, was studied for 6CB). For 8CB, on the other hand, the coefficient α_3 is found to be positive at temperatures just above the smectic phase, diminishing gradually with increasing

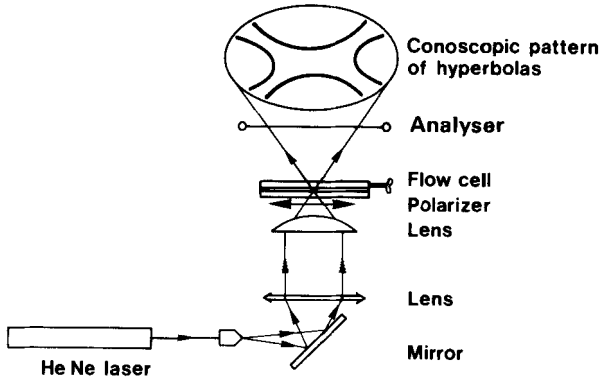

Figure 3. Conoscopic optical arrangement for the observation of the sign of α_3. A beam from a He–Ne laser is expanded and incident on the sample through a strong positive lens to produce a highly divergent beam. The sample, with the director oriented parallel to the shear velocity, is viewed between crossed polarizers. With no shear the characteristic interference pattern of hyperbolas for a uniaxial crystal is seen. When given a shear pulse, the pattern will move in either of the two directions corresponding to figures 2(*b*) and (*c*).

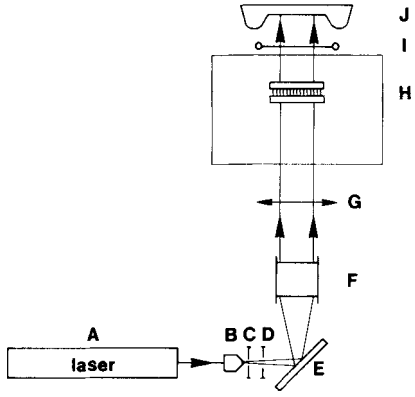

Figure 4. The torsional shear flow set-up. A laser beam, expanded through a microscope lens B, a spatial filter C and a lens D, is deflected by a mirror E and made parallel by a condenser F. Interference patterns generated by the liquid crystal sample H when viewed in the parallel laser beam between crossed polarizers G and I are recorded directly on photographic film J.

temperatures and changing sign one degree below the nematic–isotropic phase transition. This means that 8CB has a conveniently placed temperature region between 33·5°C and 39·1°C where α_3 is positive, and an intricate flow behaviour may be expected as explained in the Introduction.

The quantitative study of the flow of 8CB for positive α_3 was made in a torsional shear apparatus of the type first introduced by Wahl and Fischer [20]. The experimental set-up is shown schematically in figure 4. The nematic layer is held between two circular glass plates (diameter 50 mm). The layer thickness can be varied using three micrometers, and the parallelism of the plates is checked optically by observing interference fringes in the empty cell. The lower plate is rotated by a synchronous ten-step gear motor, giving a rotation speed for the lower plate between one

revolution in 4·8 min and one revolution in 80 hours. Along the axis of rotation an expanded He–Ne laser beam (wavelength $\lambda_0 = 632{\cdot}8$ nm) is incident on the liquid crystal layer from below. The cell is mounted between crossed polarizers, and optical patterns in the sheared liquid crystal are viewed from above in the parallel laser light beam.

The nematic is drawn into the cell by capillary action. To apply an a.c. electric field across the layers, the two glass plates have their inner surfaces coated with a very thin conducting film of tin oxide. The desired boundary conditions for the director (normal to the plates) are achieved by applying a thin layer of lecithin to the glass surfaces. When the lower plate is not rotating, we have therefore a nematic mono-domain with the director everywhere perpendicular to the plates. Viewed from above in the parallel laser light, the cell is dark (extinction between crossed polarizers). The interference patterns in the flow condition are recorded directly onto a photographic film, using a Pentax 6 × 7 mirror reflex camera housing.

For very low shear rates (10^{-3}–$10^{-2}\,s^{-1}$) the director profile in the liquid crystal layer is determined by the balance of elastic and viscous torques acting on the director. At higher shear rates (10^{-1}–$1\,s^{-1}$) the viscous torques dominate in the bulk, and the flow behaviour is critically dependent on the sign of α_3.

$\alpha_3 < 0$: Since the shear-induced birefringence increases radially outwards, an interference pattern of concentric dark rings is observed. This is the case for $\alpha_3 < 0$ even at high shear rates since flow alignment occurs.

$\alpha_3 > 0$: At low angular velocities there is no qualitative difference to the case with α_3 negative, since elastic torques balance the destabilizing viscous torques. However, at higher shear rates there is no flow alignment for $\alpha_3 > 0$. Instead new, very regular director patterns are observed.

When the rotation of the lower plate is started at the highest angular velocity ($\omega = 2{\cdot}18 \times 10^{-2}\,s^{-1}$), dark rings are observed moving in slowly. These rings are not interference rings (confirmed by observations made without analyser), but are believed to be walls separating regions of different director configuration. When the rotation has lasted for 70 s, the appearance of the cell is as in figure 5 for 8CB at 36°C. If the rotation is stopped, and an a.c. field of 50 V is applied for a few seconds across the sample, very regular concentric dark rings appear as shown in figure 6. The application of an electric field seems to develop a picture of the director in the cell, in the sense that some areas (the dark rings) will have a flow induced director profile that the field easily orients to the original, homeotropic condition. Other areas (the bright rings) will have aligned in such a way that the resulting structure scatters light intensity.

In the present work we restrict ourselves to study the first tumbling, i.e. the boundary between the central dark disc and the first bright ring in figure 6. We perform this investigation very near the nematic–smectic A transition, where $\alpha_3 \gg |\alpha_2|$. Our aim is to begin to establish a model for the observed, intriguing flow patterns that is firmly based on the Leslie–Ericksen continuum theory for nematics.

3. The tumbling instability

Experimentally it is well established that when (under the proper circumstances) a shear flow experiment is performed according to figure 1, at a certain shearing rate the director profile undergoes a discontinuous transition from one stationary state to another, provided that the Leslie viscosity α_3 is positive; this instability is called a tumbling instability. In figure 7 we sketch the outcome of a typical tumbling

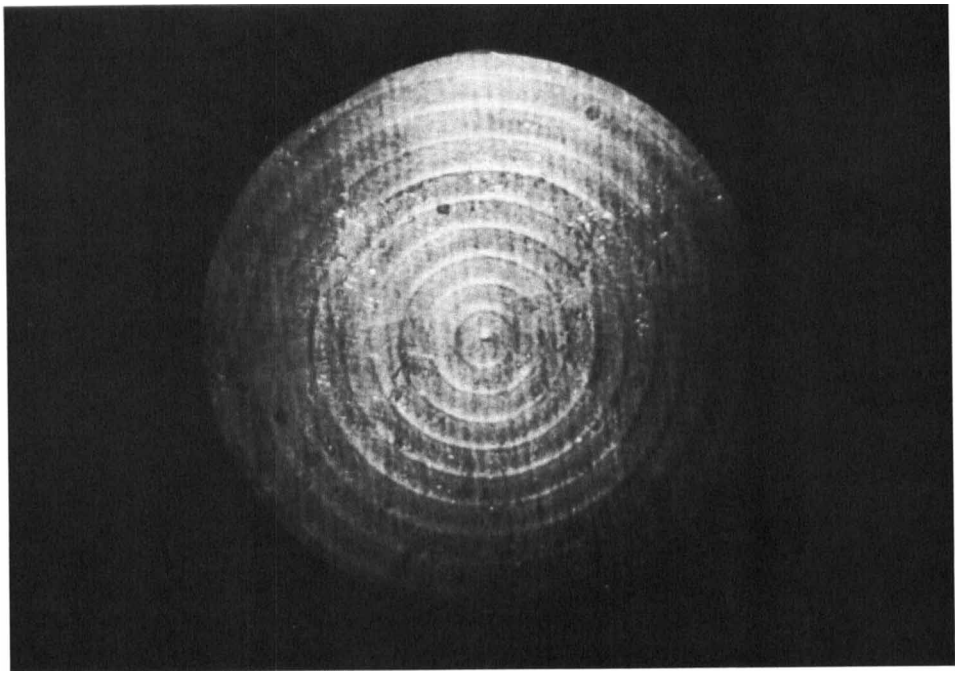

Figure 5. The appearance of the liquid crystal cell after 70 s torsional shear (angular velocity $\omega = 2{\cdot}18 \times 10^{-2} s^{-1}$). The cell thickness is 650 μm and the temperature is 36°C.

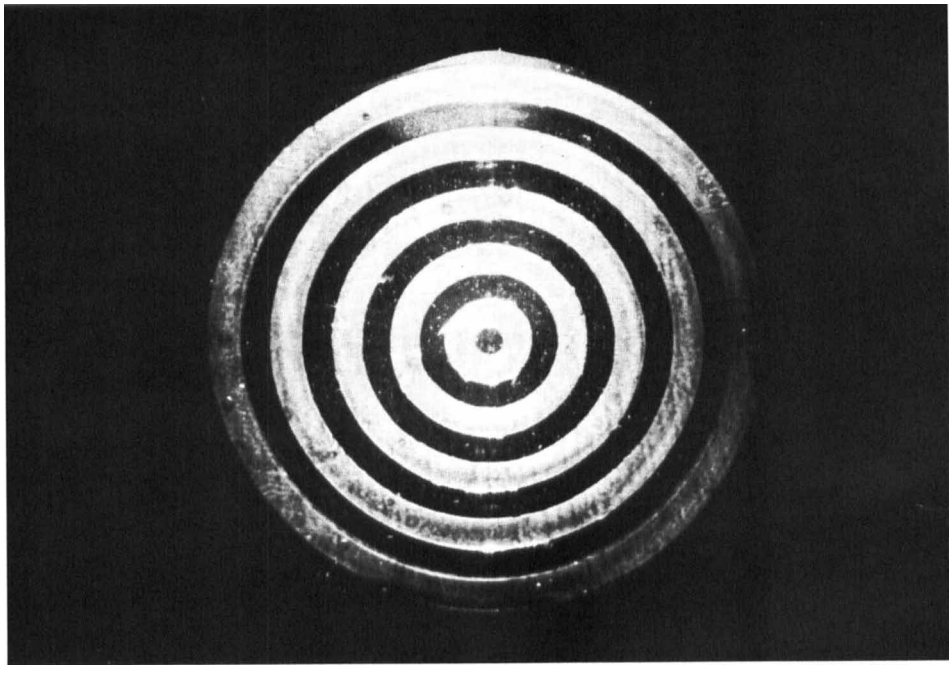

Figure 6. The appearance of the cell after stopping the shear and applying an a.c. electric field of 50 V.

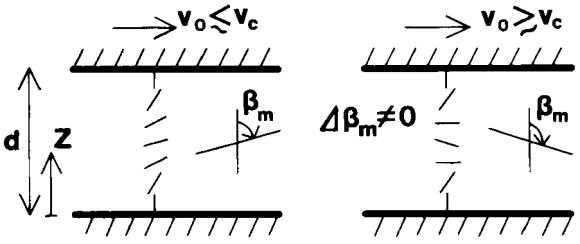

Figure 7. Tumbling of a nematic liquid crystal in shear flow. When the velocity v_0 of the moving plate increases above the critical velocity v_c, the director profile makes a discontinuous jump from one state to another. When this happens the maximum deflection of the director β_m makes a finite jump.

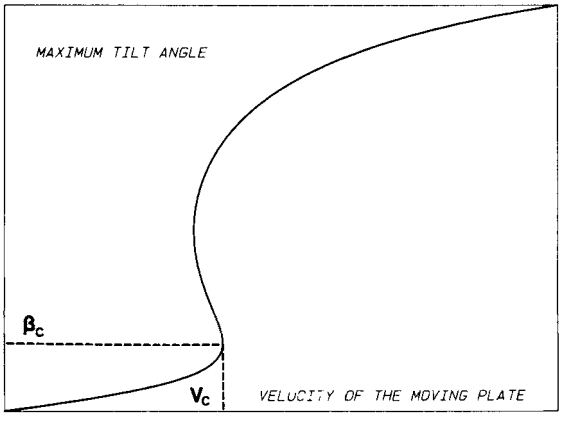

Figure 8. Calculated [18] maximum tilt angle β_m as function of the velocity v_0 of the moving plate. By increasing the velocity of the moving plate we ultimately come to a situation where β_m is forced to make a discontinuous jump. This is the tumbling instability. The tumbling angle is denoted β_c and the corresponding velocity v_c.

experiment. The liquid crystal is confined between two parallel glass plates distance d apart, one of which is moving with velocity v_0. The same boundary conditions are used on both plates, either perpendicular or parallel, the director in the latter case pointing in the x direction. For shearing rates small enough for our purpose, the director will remain within the plane of shear throughout the experiment [19]. The balance of the elastic and the shearing torques results in some director profile, $\beta(z)$, where β is the angle of deflection of the director (i.e. $\beta = \theta$ for perpendicular boundary conditions and $\beta = \theta - \pi/2$ for parallel boundary conditions). Due to the symmetry of the problem, the director profile will be symmetric around the midplane of the sample, making the maximum tilt angle, β_m, for $z = d/2$. By increasing the velocity of the moving plate the director profile will be continuously deformed, exhibiting larger values of β_m. At a critical shearing rate however, the system undergoes a discontinuous transition between two states. In this transition the maximum tilt angle makes a jump which is of the order of several tens of degrees.

A theoretical analysis of the tumbling instability has been performed by Carlsson [18], who solved the equations governing the flow numerically. Figure 8 shows the typical outcome of such a calculation. Plotted is the graph of the maximum tilt angle

β_m as function of the velocity v_0 of the moving plate. For some velocities this function is triple-valued. By a study of the entropy production of the system it can be proved that it is the lower branch which has the least entropy production and thus should be the physically most stable. By increasing the velocity of the moving plate, the system ultimately comes to a situation where β_m is forced to make a discontinuous jump; this is the tumbling instability. The value of the maximum tilt angle when tumbling occurs is called the tumbling angle and is denoted by β_c. The corresponding velocity of the moving plate is denoted by v_c. It is of major importance for the understanding of the tumbling instability to derive β_c and v_c as functions of the material parameters of the nematic as well as of the boundary conditions being used in the experiment. This problem has been studied by Högfors and Carlsson [19], who show that the crucial parameter determining the tumbling threshold is the ratio $\alpha_3/|\alpha_2|$ which we denote here by ξ. The results of Högfors and Carlsson are now summarized for perpendicular and parallel boundary conditions.

$\xi \gg 1$: *perpendicular boundary conditions*

Tumbling occurs for small tumbling angles. The tumbling angle decreases with an increasing value of ξ. When $\xi \gtrsim 10$ the approximate relations

$$v_c d = 4{\cdot}8 \frac{K_3}{\sqrt{(\alpha_3|\alpha_2|)}}, \quad \beta_c = 1{\cdot}3 \sqrt{\left(\frac{|\alpha_2|}{\alpha_3}\right)} \tag{2}$$

hold.

$\xi \gg 1$: *parallel boundary conditions*

Tumbling occurs for a tumbling angle which is slightly larger than 90°. The larger ξ is the closer to 90° is the tumbling angle.

$\xi \approx 1$: *parallel or perpendicular boundary conditions*

No tumbling occurs.

$\xi \ll 1$: *parallel boundary conditions*

Tumbling occurs for small tumbling angles. The tumbling angle decreases with a decreasing value of ξ. When $\xi \lesssim 0{\cdot}1$ the approximate relations

$$v_c d = 4{\cdot}8 \frac{K_1}{\sqrt{(|\alpha_2|\alpha_3)}}, \quad \beta_c = 1{\cdot}3 \sqrt{\left(\frac{\alpha_3}{|\alpha_2|}\right)} \tag{3}$$

hold.

$\xi \ll 1$: *perpendicular boundary conditions*

Tumbling occurs for a tumbling angle which is slightly larger than 90°. The smaller ξ is the closer to 90° is the tumbling angle.

It is easy to understand how the periodic structures which are discussed in §2 as a consequence of tumbling can be explained. The liquid crystal used in this experiment was 8CB which for the temperatures used exhibits a positive α_3 in the regime where $\xi \ll 1$. In torsional shear flow the shearing rate increases radially outwards, so at the same time a large range of shearing rates is covered (cf. figure 9). At some critical radii the shearing rate equals the critical one for tumbling. Just inside and outside such a critical radius the values of β_m predicted by the solution of the equations governing the system differ considerably. For torsional shear flow, of course, elasticity will relax the system, thus creating twist walls situated at the critical radii. These twist walls are actually seen in the experiment (cf. figure 5).

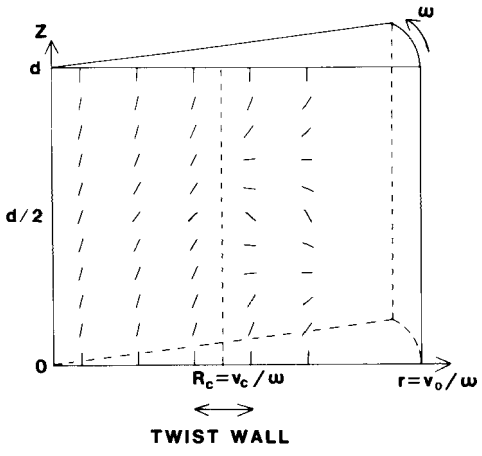

Figure 9. Schematic picture of the creation of twist walls in torsional shear flow when $\alpha_3 > 0$. The shearing rate increases linearly outwards and adopts the critical 'tumbling value' v_c at the distance R_c from the centre. Just inside and outside this radius the Leslie–Ericksen equations predict a value of the maximum tilt angle β_m which differs by a finite value. The system is then relaxed by elastic torques thus creating a twist wall at $r = R_c$. Note that the figure is schematically drawn: the tilt of the molecules shall be imagined to be perpendicular to the paper as the molecules in torsional shear flow are tilted in such a way that they are contained in the tangential plane of the cylinder with the proper radius (= the distance of the molecules to the centre), the axis of the cylinder coinciding with the symmetry axis of the experimental set-up.

The temperature dependence of ξ for 8CB is such that at low temperatures, near the nematic–smectic A phase transition, it diverges. Raising the temperature of the system ξ decreases, ultimately going through zero at which temperature α_3 changes sign and becomes negative [21, 22]. This ensures that both the limits $\xi \gg 1$ and $\xi \ll 1$ are accessible experimentally. In the work presented in [15] the experiment was performed for one arbitrary temperature in the regime $\xi \ll 1$. In this paper we perform a series of experiments for different temperatures, ξ all the time being in the regime $\xi \gg 1$. In the following section we give the experimental details and in §5 we show that by solving the equations governing the flow we are able to predict the critical radius for which the first tumbling line occurs.

4. The present experiment

In this section we study the director behaviour until the first tumbling sets in, as illustrated in figure 7. The nematic 8CB was studied very close to the smectic A–nematic transition temperature (33·5°C). In this region α_3 is positive, and moreover $\alpha_3 \gg |\alpha_2|$. As discussed in §3, this means that the director will be tilted, by a rather small angle ($\lesssim 30°$) from the homeotropic initial orientation before tumbling occurs. A small director tilt means a small effective optical anisotropy leading to a more easily resolved and evaluated optical interference pattern.

To discuss optical interference of polarized light in the flowing nematic, consider the director field shown in figure 10(*a*) which is typically obtained in a shear flow experiment. The nematic is a birefringent uniaxial medium characterized optically by the ordinary (n_0) and extra-ordinary (n_e) refractive indices ($n_e > n_0$). The director $\hat{\mathbf{n}}$ is assumed to be equivalent to the local optic axis, as shown in figure 10(*b*). The light

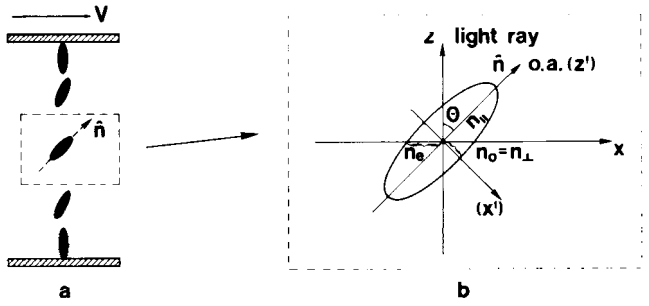

Figure 10. (*a*) Schematic picture of the director profile in the sheared nematic. (*b*) Definition of optical quantities. The light is incident along the z axis and the shear velocity is along the x axis. The director $\hat{\mathbf{n}}$ is the local optic axis (o.a.). The director makes an angle θ with the z axis.

is incident along the z axis (normal incidence), and the optic axis makes an angle θ with this axis. The projection of the index ellipsoid shown has a long axis $n_\parallel$ (along z') and a short axis $n_\perp = n_0$ (along x'). The equation for the index ellipse is

$$\frac{z'^2}{n_\parallel^2} + \frac{x'^2}{n_\perp^2} = 1. \tag{4}$$

The quantity observed experimentally is the effective optical anisotropy $n_e(\theta) - n_0$. To obtain this, we express the index ellipse in the xz coordinates through the relations

$$\left.\begin{aligned} x' &= x\cos\theta + z\sin\theta, \\ z' &= z\cos\theta - x\sin\theta. \end{aligned}\right\} \tag{5}$$

Insertion of this into equation (4) gives

$$\left(\frac{z^2}{n_\parallel^2} + \frac{x^2}{n_\perp^2}\right)\cos^2\theta + \left(\frac{z^2}{n_\perp^2} + \frac{x^2}{n_\parallel^2}\right)\sin^2\theta + \left(\frac{1}{n_\perp^2} - \frac{1}{n_\parallel^2}\right)2xz\cos\theta\sin\theta = 1. \tag{6}$$

The extraordinary refractive index is the interception between the x axis and the ellipse ($z = 0$, $x = n_e$) yielding

$$\frac{n_e^2}{n_\perp^2}\cos^2\theta + \frac{n_0^2}{n_\parallel^2}\sin^2\theta = 1, \tag{7}$$

or

$$n_e(\theta) - n_0 = n_\perp\left[\frac{1}{\sqrt{\{1 - [1 - (n_\perp^2/n_\parallel^2)]\sin^2\theta\}}} - 1\right]. \tag{8}$$

To determine the mean optical anisotropy we integrate across the sample

$$\langle n_e - n_0\rangle = \frac{2}{d}\int_0^{d/2}(n_e(\theta) - n_0)\,dz. \tag{9}$$

The function $\theta(z)$ is given by solving the hydrodynamic equations as discussed in detail in the following section.

The phase difference δ between the extraordinary and the ordinary light ray is

$$\delta = \frac{2\pi}{\lambda_0}\langle n_e - n_0\rangle d, \tag{10}$$

where $\lambda_0 = 632{\cdot}8$ nm is the wavelength of the incoming laser light beam and d is the thickness of the liquid crystal layer. The extinction condition when the sample is viewed between crossed polarizers is

$$\delta = 2\pi m. \tag{11}$$

In the torsional shear flow apparatus, because of the circular symmetry, the interference pattern will have the form of concentric dark rings, and m denotes the ring number, beginning with $m = 0$ at the centre. Finally, we find

$$\frac{m}{d} = \frac{\langle n_e(\theta) - n_0 \rangle}{\lambda_0} \tag{12}$$

making it possible to relate a shear induced director deformation $\theta(z)$ to a certain ring number m for a given liquid crystal sample with known values of $n_\parallel$ and $n_\perp$. In the present context, we are interested in $\theta(z)$, and the corresponding ring number m_c, at the critical shear rate where the first tumbling occurs. The critical shear rate corresponds in the torsional shear flow apparatus to a critical radius R_c. A typical appearance of the sample after 90 min torsional shear is shown in figure 11.

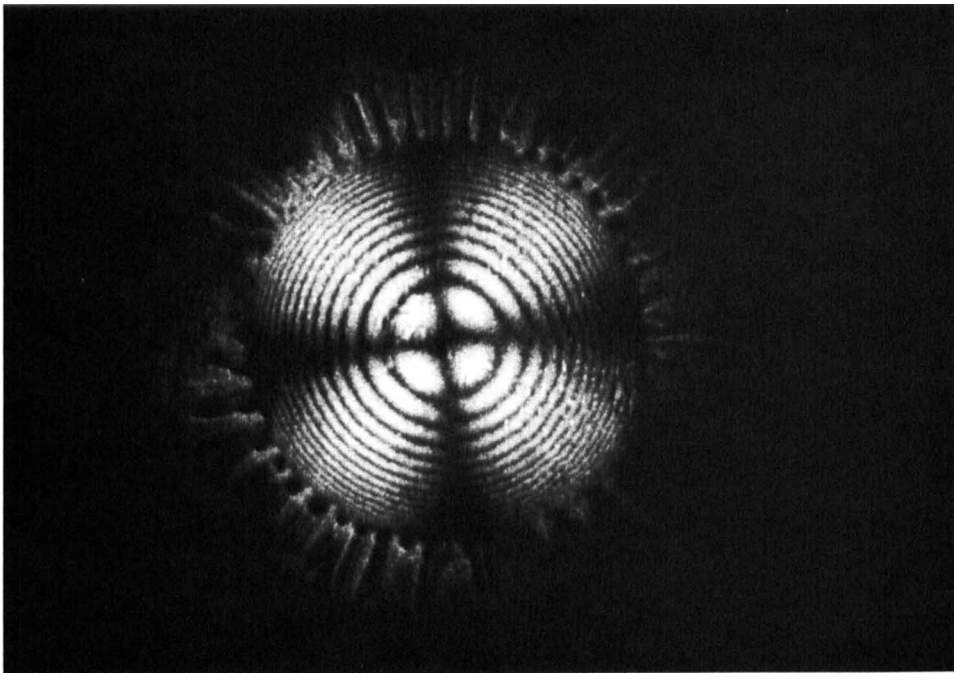

Figure 11. Photograph showing the critical radius where the first tumbling takes place ($T = 33{\cdot}78$°C).

Experimentally, it is important to establish that the observation of R_c and m_c at a certain temperature is made in a steady-state situation for the director. In figure 12 we show a plot of R_c versus time; it is seen that after about 30 min the critical radius is time-independent. A sample of thickness $d = 600\,\mu$m was prepared with 8CB. The tumbling instability was studied near the nematic–smectic A transition, in the temperature range 33·5°C to 33·8°C. In this region $\alpha_3 \gg |\alpha_2|$. Photographic pictures

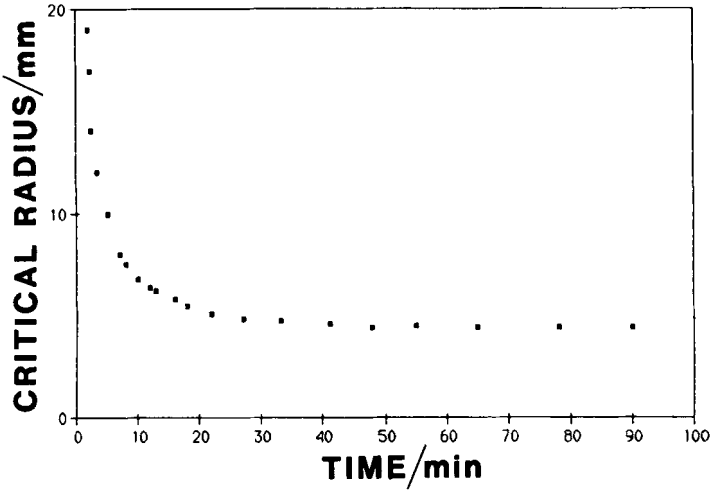

Figure 12. The critical radius for tumbling R_c as a function of time. Observation of R_c was normally done after 1 hour, when the tumbling boundary had relaxed to its stationary state.

similar to figure 11 were taken at six temperatures in this region, and analysed for R_c and m_c. In this experiment an angular velocity of the lower plate of $4{\cdot}4 \times 10^{-4} s^{-1}$ was used. Since $R_c\omega/d$ gives the critical shear rate for tumbling, and m_c can be related to the director profile $\theta(z)$ through the optical formula, we are now in a position to evaluate the experimental observation of the tumbling in terms of the predictions of the Leslie–Ericksen continuum description. This is the purpose of the following section.

5. Theoretical analysis

The distribution of the dark interference rings of figure 11 can be calculated from equations (9) and (12) provided that the director profile $\theta(z)$ is known. The task of calculating $\theta(z)$ has been solved [18, 23] and we now summarize the results of these calculations.

The equations governing the director profile $\theta(z)$ and the velocity profile $v(z)$ in the stationary state are given by

$$h(\theta)\frac{d^2\theta}{dz^2} + \tfrac{1}{2}h'(\theta)\left(\frac{d\theta}{dz}\right)^2 + (\alpha_3\sin^2\theta - \alpha_2\cos^2\theta)\frac{dv}{dz} = 0, \tag{13}$$

$$\frac{dv}{dz} = \frac{\tau}{\eta_2 - (\alpha_2 + \alpha_3)\cos^2\theta}. \tag{14}$$

Equation (13) expresses the balance of elastic and viscous torques while equation (14) is the Navier–Stokes equation applied to the present problem. The function $h(\theta)$ depends on the elastic splay and bend constants, K_1 and K_3, according to

$$h(\theta) = K_1\sin^2\theta + K_3\cos^2\theta, \tag{15}$$

while η_2 is one of the Miesowicz viscosities

$$\left.\begin{aligned}\eta_1 &= \tfrac{1}{2}(-2\alpha_2 - \alpha_3 + \alpha_4 + \alpha_6),\\ \eta_2 &= \tfrac{1}{2}(\alpha_3 + \alpha_4 + \alpha_6),\\ \eta_3 &= \tfrac{1}{2}\alpha_4\end{aligned}\right\} \tag{16}$$

and τ is the shearing force per unit area acting on the moving plate, the velocity of which is assumed to be v_0. In equation (14) we have also made the approximation $\alpha_1 = 0$, an approximation which is justified in [18]; this approximation was first suggested by MacSithigh and Currie [24]. Assuming homeotropic boundary conditions we solve equations (13) and (14) arriving at an implicit relation governing the director profile

$$z(\theta) = \frac{1}{\sqrt{(2\tau)}} \int_0^{\theta} \frac{\sqrt{[h(\theta)]}}{\sqrt{[F(\theta) - F(\theta_m)]}} d\theta, \tag{17}$$

where τ and $F(\theta)$ are given by

$$\tau = \frac{2}{d^2} \left[\int_0^{\theta_m} \frac{\sqrt{[h(\theta)]}}{\sqrt{[F(\theta) - F(\theta_m)]}} d\theta \right]^2, \tag{18}$$

$$F(\theta) = \left(\frac{\alpha_2}{\sqrt{(\eta_1 \eta_2)}} + \sqrt{\left(\frac{\eta_1}{\eta_2}\right)} \right) \arctan\left(\sqrt{\left(\frac{\eta_1}{\eta_2}\right)} \tan\theta \right) - \theta. \tag{19}$$

In these equations we have introduced the sample thickness d and the tilt in the middle of the sample $\theta_m = \theta(d/2)$, which is the maximum deflexion of the director. The velocity profile is given by

$$v(z) = \int_0^z \frac{\tau}{\eta_2 - (\alpha_2 + \alpha_3)\cos^2\theta(z)} dz. \tag{20}$$

Consequently the velocity v_0 of the moving plate is given by

$$v_0 = 2v\left(\frac{d}{2}\right) = 2 \int_0^{d/2} \frac{\tau}{\eta_2 - (\alpha_2 + \alpha_3)\cos^2\theta(z)} dz. \tag{21}$$

In a torsional shear flow experiment the velocity v_0 of the liquid crystal at the moving plate increases linearly with the distance r to the centre of the plate

$$v_0 = r\omega. \tag{22}$$

The velocity profile $\theta(z)$ for a given value of v_0 is obtained from equations (17)–(21). Substituting this into equations (8), (9) and (12) enables us to calculate the location of the dark interference rings shown in figure 11. From equations (17)–(21) we can also calculate the value of the maximum tilt angle, θ_m, as function of the velocity v_0 of the liquid crystal at the moving plate. A typical plot of $\theta_m(v_0)$ is shown in figure 8. From this we can determine the tumbling velocity v_c according to the discussion of §3. The corresponding critical radius R_c is then given as $R_c = v_c/\omega$. For a given set of material parameters α_2, α_3, α_4, α_6, K_1, K_3, $n_\parallel$ and $n_\perp$ we can therefore calculate R_c as well as the number of interference rings m_c which will be contained within the disc $r \leqslant R_c$. In this analysis we have neglected the elastic twist torque which develops because $\theta(r)$ increases radically outwards in the geometry for which the experiment is performed. It has, however, been found in the analysis of previous torsional shear flow experiments [20] that the neglect of this torque is a good approximation for the case where $\theta(r)$ is a smooth function. At $r = R_c$, where our analysis predicts $\theta(r)$ to be a step function, this torque will, of course, relax the system by creating a twist wall of a certain thickness. The crucial thing is, however, that the prediction of the location of this twist wall, which is essential for our analysis of the experiment, can be expected to be unaffected by the use of this simplified model.

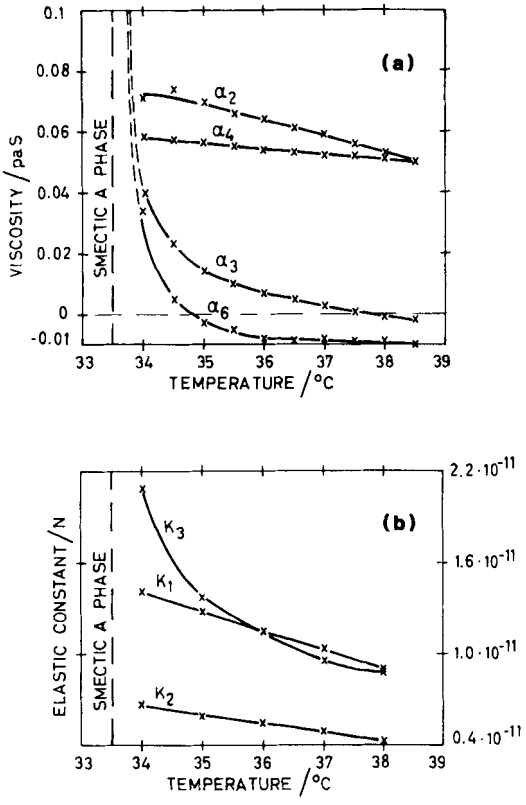

Figure 13. The viscosity coefficients (*a*) and the elastic constants (*b*) of 8CB. The data are taken from the measurements by Kneppe *et al.* [25, 26] (*a*) and Karat and Madhusudana [27] (*b*).

In order to solve equations (17)–(21) numerically we must first determine the temperature dependence of the viscosity coefficients and the elastic constants which enter the equations. Measurements of the viscosity coefficients of 8CB have been performed by Kneppe *et al.* [25, 26] while the elastic constants have been measured by Karat and Madhusudana [27]; their results are plotted in figure 13. As we are interested in the value of the material parameters in the temperature interval between 33·5°C and 33·8°C we notice however that no experimental data are available and so we have to extrapolate the graphs as the smectic A phase is approached. The viscosity coefficients, α_2 and α_4, are seen to exhibit a weak temperature dependence in the temperature interval of interest while α_3 and α_6 are seen to diverge as the smectic A–nematic transition temperature T_{S_AN} is approached. This is in accord with other experimental observations [21, 22] as well with theoretical predictions [28, 29]. We make therefore the following assumptions

$$\alpha_2 = -0{\cdot}07\,\text{Pa s},$$

$$\alpha_3 = \xi\,\alpha_2|,$$

$$\alpha_4 = 0{\cdot}06\,\text{Pa s},$$

$$\alpha_6 = \alpha_3.$$

The ratio $\xi = \alpha_3/|\alpha_2|$ is assumed to diverge according to some critical exponent γ as the temperature approaches T_{S_AN}. The value of γ is however immaterial for our purpose. Of the elastic constants we are only interested in K_1 and K_3. Of these K_1 is almost constant close to T_{S_AN} while K_3 exhibits a critical divergence [30, 31]. To make the simplest possible assumption we take the critical exponent of the divergence of $\kappa = K_3/K_1$ to be the same as that of ξ and write

$$\xi = \xi_0(T - T_{S_AN})^{-\gamma}, \tag{23}$$

$$\kappa = \kappa_0(T - T_{S_AN})^{-\gamma}. \tag{24}$$

From equations (23) and (24) we find

$$\kappa = \frac{\kappa_0}{\xi_0}\xi. \tag{25}$$

In figure 13 we see that at the temperature where $\xi = 1$, the value of κ is approximately 1·65. This suggests to us that κ_0/ξ_0 is 1·65 and the assumption made for the elastic constants is

$$K_1 = 1{\cdot}45 \times 10^{-11}\,\mathrm{N},$$

$$K_3 = 1{\cdot}65\,\xi K_1.$$

We further need the values of the refractive indices $n_\perp$ and $n_\parallel$ close to the phase transition. These have been measured by Karat and Madhusudana [32] and are found to be approximately constant in the temperature interval of interest here (wavelength of incident light, $\lambda_0 = 632{\cdot}8$ nm) with

$$n_\perp = 1{\cdot}517,$$

$$n_\parallel = 1{\cdot}666.$$

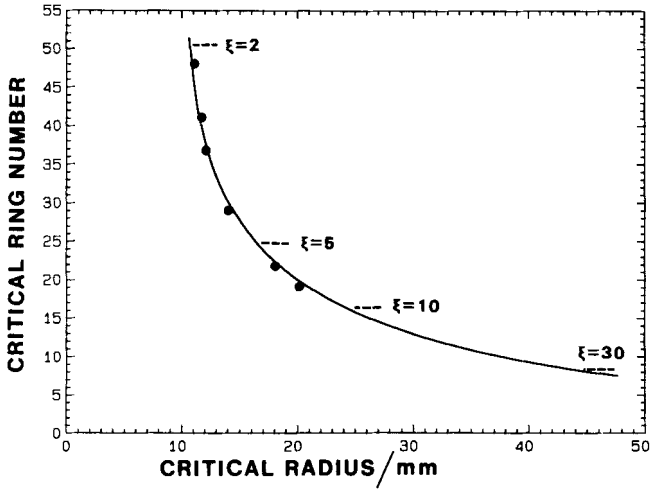

Figure 14. Critical ring number m_c as function of the critical radius $R_c = v_c/\omega$ for which tumbling occurs. The solid line represents the theoretical graph computed by the use of the Leslie–Ericksen hydrodynamic theory of nematics and shows how $m_c(R_c)$ varies as $\xi = \alpha_3/|\alpha_2|$ is varied from 2 to 30. The dots are the experimental data which was obtained at six different temperatures 33·51°C, 33·57°C, 33·63°C, 33·68°C, 33·71°C and 33·78°C. The temperature decreases when following the graph from left to right.

For a given value of ξ, i.e. for a given temperature, we are now in the position to calculate R_c and m_c thus giving us the functional dependence $m_c(R_c)$ parametrized by ξ. The outcome of such a calculation is shown by the solid line in figure 14; in this graph $\xi = 2$ in the upper left part increasing to the value $\xi = 30$ in the lower right part. The dots in the same figure represent the measured values of m_c and R_c for the six temperatures 33·51°C, 33·57°C, 33·63°C, 33·68°C, 33·71°C and 33·78°C following the graph from right to left. We note the good agreement between the experimental points and the theoretically calculated curve.

6. Discussion

In the present work we have studied the torsional shear flow in a nematic with $\alpha_3 > 0$, and in addition $\alpha_3/|\alpha_2| \gg 1$. In this regime tumbling occurs for small tilt angles. This makes the experiment easier and more accurate than for the $\alpha_3/|\alpha_2| \ll 1$ regime, where tumbling occurs for tilt angles slightly above $\pi/2$. In both cases we refer to perpendicular boundary conditions. The reason is that the effective optical anisotropy $\langle n_e(\theta) - n_0 \rangle$ in the former case is much smaller, and thus the critical ring number m_c is smaller. For m_c of 100, as in the $\alpha_3/|\alpha_2| \ll 1$ regime, the density of interference fringes is very high, and consequently the accuracy with which m_c can be determined decreases.

The special case $\alpha_3/|\alpha_2| = 1$ leads to a situation where no tumbling occurs. This can be seen from equations (13) and (14), which simplify in such a way that the resulting solution for θ_m as a function of the shear velocity does not show the multi-valued states leading to tumbling (cf. the curve for $T = 38$°C in figure 7 of [8].) This curve corresponds to $\xi = 0{\cdot}57$, and indicates that there is an interval around $\xi = 1$ (and a corresponding temperature interval) where tumbling does not occur.

As can be seen from equation (2), the elastic torques become more important relative to the shear torque near the nematic–smectic A transition. This means that the critical radius R_c, where tumbling occurs, should increase with increasing value of ξ since K_3 and α_3 are assumed to diverge homomorphically at the phase transition. This behaviour is also observed as is indicated in figure 14. The effect can be observed to its full extent in the smectic A phase itself, where it was not possible experimentally even with the highest shear rate to induce any deformation of the homeotropic director.

As we have discussed in the Introduction, Pieranski *et al.* [13] reported the linear shear flow of nematics with positive α_3 to be unstable with respect to fluctuations which bring the director out of the shearing plane. The fact that we observe a sequence of walls as shown in figure 6 shows that the out-of-plane instability does not occur in torsional shear flow; this can be understood using an argument due to Chandrasekhar [33]. In torsional shear flow the liquid crystal is confined between two parallel, circular glass plates; one at rest while the other one is rotating. If the instability threshold is reached the director would start to rotate out of the plane of shear. This sudden rotation is coupled to a hydrodynamic flow, commonly called back flow [34]. In this case the back flow would be radial, thus creating a pressure drop in the centre of the sample. This pressure drop would suppress the back flow and thereby act to stabilize the director against fluctuations out of the plane of shear.

References

[1] Oseen, C. W., 1929, *Fortschr. Chem Phys. phys. Chem.*, **20**, 25.
[2] Anzelius, A., 1931, *Uppsala Univ. Årsskr. Mat. och Naturvet.*, p. 1.

[3] ERICKSEN, J. L., 1960, *Archs ration. Mech. Analysis*, **4**, 231.
[4] LESLIE, F. M., 1968, *Archs ration. Mech. Analysis*, **28**, 265.
[5] LESLIE, F. M., 1968, *Proc. R. Soc.* A, **307**, 359.
[6] PARODI, O., 1970, *J. Phys., Paris*, **31**, 581.
[7] CARLSSON, T., 1986, *Phys. Rev.* A, **34**.
[8] CARLSSON, T., 1982, *Molec. Crystals liq. Crystals*, **89**, 57.
[9] CARLSSON, T., 1983, *J. Phys., Paris*, **44**, 909.
[10] CLADIS, P. E., and TORZA, S., 1975, *Phys. Rev. Lett.*, **35**, 1283.
[11] CLADIS, P. E., and TORZA, S., 1976, *Colloid and Interface Science*, Vol. IV (Academic Press), p. 487.
[12] PIERANSKI, P., and GUYON, E., 1974, *Phys. Rev. Lett.*, **32**, 924.
[13] PIERANSKI, P., GUYON, E., and PIKIN, S., 1976, *J. Phys., Paris*, Colloq., **37**, C1, 3.
[14] CLARK, M. G., SAUNDERS, F. C., SHANKS, I. A., and LESLIE, F. M., 1981, *Molec. Crystals liq. Crystals*, **70**, 195.
[15] SKARP, K., CARLSSON, T., DAHL, I., LAGERWALL, S. T., and STEBLER, B., 1980, *Advances in Liquid Crystal Research and Applications*, edited by L. Bata (Pergamon Press), pp. 573–581.
[16] PIKIN, S. A., 1974, *Sov. Phys. JETP*, **38**, 1246.
[17] MANNEVILLE, P., 1981, *Molec. Crystals liq. Crystals*, **70**, 223.
[18] CARLSSON, T., 1984, *Molec. Crystals liq. Crystals*, **104**, 307.
[19] HÖGFORS, C., and CARLSSON, T., in CARLSSON, T., 1984, Dissertation, Chalmers University of Technology, Göteborg.
[20] WAHL, J., and FISCHER, F., 1973, *Molec. Crystals liq. Crystals*, **22**, 359.
[21] PIERANSKI, P., and GUYON, E., 1976, *Commun. Phys.*, **1**, 45.
[22] SKARP, K., CARLSSON, T., LAGERWALL, S. T., and STEBLER, B., 1981, *Molec. Crystals liq. Crystals*, **66**, 199.
[23] CURRIE, P. K., and MACSITHIGH, G. P., 1980, *Q. Jl Mech. appl. Math.*, **32**, 499.
[24] MACSITHIGH, G. P., and CURRIE, P. K., 1977, *J. Phys.* D, **10**, 1471.
[25] KNEPPE, H., SCHNEIDER, F., and SHARMA, N. K., 1981, *Ber. Bunsenges. phys. Chem.*, **85**, 784.
[26] KNEPPE, H., SCHNEIDER, F., and SHARMA, N. K., 1982, *J. chem. Phys.*, **77**, 3203.
[27] KARAT, P. P., and MADHUSUDANA, N. V., 1977, *Molec. Crystals liq. Crystals*, **40**, 239.
[28] JÄHNIG, F., and BROCHARD, F., 1974, *J. Phys., Paris*, **35**, 301.
[29] MCMILLAN, W. L., 1974, *Phys. Rev.* A, **9**, 1720.
[30] DE GENNES, P. G., 1972, *Solid St. Commun.*, **10**, 753.
[31] CHEUNG, L., MEYER, R. B., and GRULER, H., 1973, *Phys. Rev. Lett.*, **31**, 349.
[32] KARAT, P. P., and MADHUSUDANA, N. V., 1976, *Molec. Crystals liq. Crystals*, **36**, 51.
[33] CHANDRASEKHAR, S. (personal communication).
[34] CHANDRASEKHAR, S., 1977, *Liquid Crystals* (Cambridge University Press), p. 152.